RSC Advances

Novel La3GaGe5O16:Mn4+ Based Deep Red Phosphor: A Potential Color Converter for Warm White Light

Journal:	*RSC Advances*
Manuscript ID	RA-ART-09-2015-018163.R1
Article Type:	Paper
Date Submitted by the Author:	13-Oct-2015
Complete List of Authors:	Zhang, Shaoan; Guangdong University of Technology, School of Physics and Optoelectronic Engineering Hu, Yihua; Guangdong University of Technology, School of Physics and Optoelectronic Engineering Duan, He; Guangdong University of Technology, School of Physics and Optoelectronic Engineering Chen, Li; Guangdong University of Technology, School of Physics and Optoelectronic Engineering Fu, Yinrong; Guangdong University of Technology, School of Physics and Optoelectronic Engineering Ju, Guifang; Guangdong University of Technology, School of Physics and Optoelectronic Engineering Wang, Tao; Guangdong University of Technology, School of Physics and Optoelectronic Engineering
Subject area & keyword:	Optical materials < Materials

Novel $La_3GaGe_5O_{16}:Mn^{4+}$ Based Deep Red Phosphor: A Potential Color Converter for Warm White Light

Shaoan Zhang, Yihua Hu*, He Duan, Li Chen, Yinrong Fu, Guifang Ju, Tao Wang, and Miao He

School of Physics and Optoelectronic Engineering, Guangdong University of Technology, Waihuan Xi Road, No.100, Guangzhou 510006, People's Republic of China.

Abstract:

New non-rare-earth red phosphor $La_3GaGe_5O_{16}:Mn^{4+}$ was prepared successfully via the traditional solid state reaction method. In this paper, we reported this red phosphor $La_3GaGe_5O_{16}:Mn^{4+}$ as a promising red converter for warm white light under excitation at UV or blue light. The phase and microstructure of this red phosphor were characterized with aids of the XRD and SEM; the luminescent performance was investigated by the diffuse reflection spectra, photoluminescence (PL) spectra, and temperature-dependent PL/decay measurements. The excitation band of $La_3GaGe_5O_{16}:Mn^{4+}$ phosphor covers a broad spectral region from 250 nm to 500 nm, which match well with the commercial near-UV and blue LEDs and can give intense bright red emission. The crystal field strength (Dq) and the Racah parameters (B and C) are calculated to evaluate the nephelauxetic effect of Mn^{4+} suffering from the $La_3GaGe_5O_{16}$ host. The concentration quenching of Mn^{4+} in $La_3GaGe_5O_{16}:Mn^{4+}$ occurs at a low content of 0.25% due to the dipole-dipole interaction in this work. We gained insight into the temperature-dependent relative emission intensity of $La_3GaGe_5O_{16}:0.25\%Mn^{4+}$ phosphor, and we also reported the luminescence quenching temperature and the activation energy for thermal quenching (ΔE). In

future, WLEDs will be made when this red phosphor was applied to the package of a UV/blue LED chip and YAG:Ce.

Key word: Optical phosphor; Deep-red emission ; Mn^{4+}-doped; $La_3GaGe_5O_{16}$ host

Corresponding Author

Tel.:+86-020-39322262;

Fax: +86-020-39322265

E-mail address: huyh@gdut.edu.cn (Yihua Hu)

1. Instruction

Over the past decades, the white light-emitting diodes (WLEDs) has been the most promising light source in general lighting and displays field due to their admirable merits such as energy efficiency, reasonable cost, long lifetime, and environmental friendliness [1-5]. In recent years, a vast number of papers gave the detailed descriptions for different methods of creating white light [4-8]. However, the current leading commercial WLEDs is the conjunction of an InGaN chip and a yellow-emitting $Y_3Al_5O_{12}:Ce^{3+}$ (YAG:Ce) phosphor, *i. e.*, the yellow phosphor YAG:Ce dispersed in epoxy or silicone is directly packed on the blue InGaN chip [9-10]. Unfortunately, such design in practical application suffers some technical weakness. One primary problem is the innate deficiency in red components, resulting in poor rendering ability and a high correlated color temperature (CCT) [9-10]. To overcome the above drawbacks, it is therefore logical to supply a red phosphor into this system to improve the quality of illumination. The red phosphor should have a strong blue absorption and cann't be excitable by green light [9-12]. The idea has stimulated research on red phosphors activated by rare earth, with outstanding candidates being divalent europium-doped nitrides or oxynitrides [13-14]. But, there are obvious weakness for the Eu^{2+} and Ce^{3+} doped (oxy)nitrides ($CaAlSiN_3:Eu^{2+}$ and $M_2Si_5N_8:Ce^{3+}$ (M=Ca, Sr and Ba)) [13-14], mainly due to the critical synthetic requirement and serious photon

reabsorption phenomenon[15]. As an alternative, the non-rare-earth Mn^{4+}-doped red phosphors, which can be prepared under milder conditions, have gained increasing attention and burgeoning interest due to eco-friendly price and unique luminescent properties [16-17]. Mn^{4+} is featured by the $3d^3$ electron configurations with electrons locating in an outer orbit, which causes its optical property heavily affected by the host. In other words, the red emission of spin-forbidden $^2E_g \rightarrow {}^4A_{2g}$ depends strongly on the covalence of the Mn^{4+}-ligand bonding though the lowest excited state energy $^2E(t_2^3)$ barely changes upon variation in the crystal field. Usually, Mn^{4+} shows broad and strong absorption spanning from 300 to 480 nm and emits bright light from 600 to 760 nm when Mn^{4+} occupies an octahedral site [18-19].With regard to this merits, and as the spectroscopic properties almost ideally match the requirements, Mn^{4+} is a promising activators for red phosphors in warm WLEDs.

Although only $3.5MgO•0.5MgF_2•GeO_2:Mn^{4+}$ (MMG:Mn^{4+}) has been commercialized up to now[19], the luminescence of Mn^{4+} has been still studied in different systems. Mn^{4+} can substitutionally dissolve in fluoride compounds such as $A_2BF_6:Mn^{4+}$ (A=Li, Na, and K, B=Ge, Si, Sn), $ABF_6:Mn^{4+}$ (A=Zn, Ca, Sr and Ba,), in which Mn^{4+} exhibits an intense excitation band locating at ~460nm and sharp emission lines peaking at ~630nm. Compared with fluoride compounds, oxide compounds show much higher chemical stability with an eco-friendly preparation procedure. Peng et al recently reported a orderly-layered tetravalent manganese-doped strontium aluminate $Sr_4Al_{14}O_{25}:Mn^{4+}$ red phosphor, whose luminescent properties are superior to the commercial MMG:Mn^{4+} [18]. Novel $CaMg_2Al_{16}O_{27}:Mn^{4+}$ based red phosphor gives an excellent luminescent property in warm WLEDs [20]. Up to date, the Mn^{4+}-doped oxides, including $SrMgAl_{10}O_{17}:Mn^{4+}$ [21], $CaAl_4O_7:Mn^{4+}$ [22], $Mg_2TiO_4:Mn^{4+}$ [23] and so on, show promising capabilities as good red converters for WLEDs.

As far we know, the Mn^{4+}-doped oxides have a common ground, in which a octahedral site is occupied by Mn^{4+}. In other words, Mn^{4+} can only be accommodated and stabilized in an octahedral lattice site. This gives us a hint to explore the ideal red phosphor. Therefore, we select the Mn^{4+} ions as the activators and the gallogermanates ($La_3GaGe_5O_{16}$) as the target host due to its unique crystal structure [24]. Recently, only Xia et al. reported the photoluminescence luminescence and energy transfer behavior of $La_3GaGe_5O_{16}:Tb^{3+}$, Eu^{3+} phosphors and the near-infrared luminescence of $La_3GaGe_5O_{16}:Cr^{3+}$ phosphors [25-26]. The basic structural units are composed of [GeO_6] octahedron, [GeO_4] tetrahedron and [GaO4] tetrahedron. Each [GeO_6] octahedron is connected with six tetrahedron via common corners; every tetrahedron is linked to two octahedron forming chains of composition [$Ge(Ga,GeO_4)_3$] parallel [100]. In the b, c-plane the chains are connected by [Ge_2O_8] groups, which consist of two-edge-linked pseudo-tetragonal GeO_5 pyramids to a three dimensional framework structure with channels parallel [100], as shown in Figure 1. So, this structure can be designed to provide ideal cation sites and coordination polyhedra for manganese ion .Supposing that manganese ion could be doped into the host, it tends to substitute for germanium or gallium sites as a result of matched size and charge. To be honest, we paid our main research interests to the merits of lattice structure of $La_3GaGe_5O_{16}$ host and ignored the high price of raw materials such as La_2O_3, GeO_2 and Ga_2O_3. Indeed, a high price of the host will discourage its practical usage; but the research on this phosphor $La_3GaGe_5O_{16}:Mn^{4+}$ can enhance the system of red phosphor. The best appropriate host for Mn^{4+} is cheap, nontoxic, and environmentally-friendly such as aliminates ($SrMgAl_{10}O_{17}:Mn^{4+}$[21], $Sr_4Al_{14}O_{25}:Mn^{4+}$[18]) , and titanate ($MgTiO_4:Mn^{4+}$[23]). At later ages, we will pay more attention to the above aliminates or titanates and make effects to develop low-cost and efficient red-emitting phosphors.

In this paper, we give an insightful investigation of the luminescence of Mn^{4+}-doped $La_3GaGe_5O_{16}$ red phosphor. The photoluminescence properties of $La_3GaGe_5O_{16}$:Mn^{4+} phosphor were reported and the dependent temperature luminescence intensities and decay curves were measured. The activation energy for thermal quenching was obtained for $La_3GaGe_5O_{16}$:Mn^{4+}.

2. Experimental procedures

2.1 Synthesis

The samples were prepared by a simple solid state reaction. La_2O_3 (99.99%), Ga_2O_3 (99.99%), GeO_2 (99.99%) and $MnCO_3$ (99.99%) were used as starting materials. After the raw materials were weighed according to the composition of $La_3GaGe_5O_{16}$:$x$$Mn^{4+}$($x$=0, 0.05%, 0.15%, 0.25%, 0.35%, 0.50%, and 1%, etc), the powders were mixed and milled thoroughly for 1h in an agate mortar and prefired at 900℃ for 8h in air. After ground again, the mixtures were sintered at 1300 ℃ for 12h. After being cooled down to room temperature naturally, the as-prepared powder samples were obtained.

2.2. Characterization of samples

The phase purity of the prepared phosphors was measured by an X-ray diffractometer with Cu Ka radiation (wavelength =0.15406 nm) at 36 kV tube voltage and 20 mA tube current. The morphology of the samples was characterized by S3400N scanning electronic microscope (SEM) with accelerating voltage of 10 kV. Diffuse reflection spectra were obtained by an ultraviolet (UV)-visible spectrophotometer (Shimadzu UV-2450) using $BaSO_4$ as a reference. The photoluminescence excitation (PLE), photoluminescence (PL) emission, the temperature-dependent PL spectra and decay curves were recorded by the spectrophotometer (Edinburgh

Instrument, FLS 980) equipped with both continuous and pulsed xenon lamps (450 W) as the light source.

3. Results and discussion

3.1. Phase Characterization and morphology

The XRD patterns for all samples were examined to characterize the phase purity and crystallinity of the as-prepared powder samples. Figure 2 shows the XRD pattern of the samples $La_3GaGe_5O_{14}$ host and $La_3GaGe_{5(1-x)}O_{14}$:$x$$Mn^{4+}$($x$=0.05%, 0.15%, 0.25%, 0.35%, and 0.50%) along with ICSD card 50521 at the bottom. Evidently, all diffraction peaks are good agreement with the standard data of $La_3GaGe_5O_{14}$ (ICSD#50521). One can see that the obtained samples are single phase and the doped manganese ions are successfully dissolved into the $La_3GaGe_5O_{14}$ host lattice while maintaining the crystal structure intact. The doped Mn^{4+} ions prefer to occupy the octachhedral Ge^{4+} sites in this host because of the strong ligand-field stabilization energy of Mn^{4+} in 6-fold coordination except for the similar ionic radii between Ge^{4+} (R_{Ge4+}=0.53Å, CN=6) and Mn^{4+} (R_{Mn4+}=0.53Å, CN=6) ions[27-28].

As far we know, the morphology of desired particles has a certain influence on the luminescent behavior. So SEM of $La_3GaGe_5O_{16}$:Mn^{4+} phosphor was exhibited in Figure 3(a-d). Figure 3(a-b) illustrates that the sphere-shaped particles has a diameter of about 100 μm. Closely observing the selected part (A) of a particle at higher magnification in Fig.2 (c-d), one can see that the sphere-shaped particle consists of a number of blocked micro-grains and these grains has a length of 1-2 μm.

3.2 Photoluminescence Properties of $La_3GaGe_5O_{16}:Mn^{4+}$

Figure 4 gives the diffuse reflection spectra of $La_3GaGe_5O_{16}:Mn^{4+}$ with various Mn^{4+} doping contents. The spectrum of $La_3GaGe_5O_{16}$ host shows a platform of high reflection in the wavelength range of 400-800 nm and then starts to decrease dramatically from 400 nm to 200 nm. This band is due to the host absorption. The diffuse reflection spectra of $La_3GaGe_5O_{16}:xMn^{4+}$ (x=0.05%, 0.15%, and 0.25%) contains some absorption band corresponding to the transitions within the $3d^3$ shell of Mn^{4+} ions. The absorption band located at 330 nm is attributed to the contribution of both host absorption and the $^4A_{2g}\rightarrow{}^4T_{1g}$ transition of Mn^{4+}. Other two absorption bands at the wavelength of 467 nm and 397nm can be attributed to $^4A_{2g}\rightarrow{}^2T_{2g}$ and $^4A_{2g}\rightarrow{}^4T_{2g}$ of Mn^{4+}.

Figure 5(a) demonstrates the typical PLE (λ_{em}=660 nm) and PL (λ_{ex}=330 nm) spectra of $La_3GaGe_5O_{16}$:0.25%Mn^{4+} at room temperature. The PLE spectrum monitored at 660 nm covers a very broad spectral region from 250 nm to 550 nm. It consists of three main excitation bands originating from the d-d inner transitions of Mn^{4+}, and one can see two typical spin-allowed transitions $^4A_{2g}\rightarrow{}^4T_{1g}$ and $^4A_{2g}\rightarrow{}^4T_{2g}$ of Mn^{4+}, which peaks at ~330 nm and ~467 nm, respectively ; and a distinguishable spin-forbidden transition $^4A_{2g}\rightarrow{}^2T_{2g}$ of Mn^{4+} locates at ~397 nm. From Fig.5, we can see that $La_3GaGe_5O_{16}:Mn^{4+}$ might be less suitable for application in blue LED plus YAG:Ce system due to a relatively low absorption in blue region compared with the absorption of $La_3GaGe_5O_{16}:Mn^{4+}$ in UV region. Otherwise, some other dopant such as Bi^{3+} can be used to enhance the blue region absorption as reported in literature [23]. Thus, we plan to

enhance the blue region absorption by co-doping the Bi^{3+} ions into the $La_3GaGe_5O_{16}:Mn^{4+}$ phosphor in future.

One dominant sharp peak and two satellite peaks are found under excitation with 330nm at room temperature in Figure 5. These emissions are identified as the anti-Stokes and Stokes transitions between ^2E and $^4A_2$ levels of Mn^{4+}. Once manganese ion occupies an octahedral site, it presents the +4 valence state, shows broad and strong absorption spanning from 300 to 480 nm and emits light between 600 and 700 nm [27]. Based on the spectroscopic properties, we can conclude that Mn^{4+} probably occupies the octahedral Ge^{4+} sites in $La_3GaGe_5O_{16}$ host.

Figure 6(a) shows the schematic energy levels of Mn^{4+}, the corresponding excitation spectrum and electron transitions for the Mn^{4+} doped $La_3GaGe_5O_{16}$ phosphor is given based on the excitation spectrum measured at 10K. The energy of these excitation bands, including the 330 nm band, the 397 nm band and the 467nm band, corresponds to 30120cm^{-1}, 25189cm^{-1} and 21413cm^{-1}, respectively. Mn^{4+} belongs to $3d^3$ electronic configurations and the splitting of the energy levels in octahedral symmetry can be expressed by the well-known Tanabe-Sugano energy level diagram in Figure 6(b). The d^3 configuration gives rise to two quartet terms: ^4F and ^4P, ^4F term lying lower to ^4P as per Hund's rule. In addition to these two quartet terms, there are several doublet terms: ^2G and ^2F. The ^2G term splits into only ^2E level, and the $^4A_2$, $^4T_2$ and $^4T_1$ levels come from the ^4F term. The values of crystal-field strength (Dq) can be determined by the average peak energy of the $^4A_{2g} \rightarrow {}^4T_{2g}$ transition [29]:

$$Dq = E(^4A_{2g} \rightarrow {}^4T_{2g})/10 \quad (1)$$

On the basis of the peak difference between the $^4A_{2g} \rightarrow {}^4T_{2g}$ and $^4A_{2g} \rightarrow {}^4T_{1g}$ transitions of Mn^{4+}, the Racah parameter B can be evaluated from the expression [30]:

$$\frac{Dq}{B} = \frac{15(x-8)}{(x^2-10x)} \quad (2)$$

Where the parameter x is defined as follows:

$$x = \frac{E(^4A_{2g} \rightarrow {}^4T_{1g}) - E(^4A_{2g} \rightarrow {}^4T_{2g})}{Dq} \quad (3)$$

Based on the peak energy of $^2E_g \rightarrow {}^4A_{2g}$ (~15174 cm^{-1}) derived from the emission spectrum, the Racah parameter C can be calculated by the following expression[31]:

$$\frac{E(^2E_g \rightarrow {}^4A_{2g})}{B} = \frac{3.05C}{B} - \frac{1.8B}{Dq} + 7.9 \quad (4)$$

The values of Dq, B and C in the $La_3GaGe_5O_{16}:Mn^{4+}$ phosphors are determined to be 2141cm^{-1}, 856cm^{-1}, and 2947cm^{-1}, respectively. The values of Racah parameters (B and C) and the crystal-field strength (Dq) are similar to those reported by the $CaMg_2Al_{16}O_{27}:Mn^{4+}$ [20] or $CaAl_{12}O_{19}:Mn^{4+}$ phosphors [23].

The PLE and PL spectra of $La_3GaGe_5O_{16}:x\%Mn^{4+}$ (x=0.05, 0.15, 0.25, 0.35, and 0.50) are shown in Figure 7(a-b). Evidently, the PLE and PL spectra of $La_3GaGe_5O_{16}:x\%Mn^{4+}$ samples are almost identical except for the fluorescence intensity. The reason for this is that the activator Mn^{4+} might occupy only one octahedral site and be affected by the identical crystal-field. Furthermore, Figure 7(c) gives the Mn^{4+} content dependent PL intensities. Obviously, Mn^{4+} concentration (x) in $La_3GaGe_5O_{16}:Mn^{4+}$ phosphor reach a saturation point at x=0.25%. After that, the PL intensity begins to decrease with the Mn^{4+} content increasing due to the concentration quenching effect. Thus the optical doping concentration of Mn^{4+} is determined to be about 0.25% and the quenching concentration also can be obtained.

As for the concentration quenching phenomenon, it is due to the occurrence of energy transfer within the nearest Mn^{4+} ions followed by energy transfer to traps or quenching sites. The

involved energy transfer mechanism of $La_3GaGe_5O_{16}:Mn^{4+}$ is not radiation re-absorption since there is no overlap between PLE and PL spectra of $La_3GaGe_5O_{16}:Mn^{4+}$. So, it might be related to exchange interaction or multipole-multipole interaction. In order to know which one causes the concentration quenching, the critical distance between the neighboring Mn^{4+} ions is obtained by the following equation:

$$R_c \approx 2\times(\frac{3V}{4\pi x_c N})^{\frac{1}{3}} \quad (5)$$

where x_c is the critical concentration, N the number of available sites for the dopant in the unit cell, and V is the volume of the unit cell [32] and , the value of V and N are 611.82 $Å^3$ and 5 in the crystal lattice, respectively [24]. Supposed that the critical concentration is 0.25%, the critical distance among Mn^{4+} ions is calculated to be 68.08 Å. However, the critical distance of exchange interaction is normally around 5 Å [33], thus the exchange interaction plays little role in the energy transfer among Mn^{4+} ions because R_c is much larger than 5 Å. Therefore, the energy transfer mechanism among Mn^{4+} ions is considered as multipolar interaction. The type of the multipolar interaction can be determined based on the following equation:

$$\frac{\mathrm{I}}{x} = K\left[1+\beta(x)^{Q/3}\right]^{-1} \quad (6)$$

where I presents the integrated emission intensity, x is the concentration of activator, K and β are constants [31]. The Q is the index of electric multipole, for dipole-dipole, dipole-quadrupole, and quadrupole-quadrupole, corresponding to 6, 8, and 10, respectively. Equation (6) can be approximately simplified to be $\lg(\frac{I}{x}) = A - \frac{Q}{3}\lg x$ (Eqn. 7). As shown in Figure 7(d), the values of lg(I/x) as a function on the lg(x) are plotted. The nearly liner fitting can be obtained and the slope of the fitting line is about -2.096. So, the value of Q can be calculated to be 6.288, which reveals

that the concentration quenching of Mn^{4+} in $La_3GaGe_5O_{16}$ host is mainly due to the dipole-dipole interaction.

In order to further understand the concentration quenching in detail, the decay curves of $La_3GaGe_5O_{16}$:*x*%Mn^{4+} (*x*=0.05, 0.15, 0.25, 0.35, and 0.50) samples excited by 330 nm and monitored at 659 nm are measured and depicted in Figure 8. We can see that the decay lifetime of Mn^{4+} emission decreases faster with higher doping Mn^{4+} concentration. Obviously, the distance between Mn^{4+} ions decreases with increasing Mn^{4+} concentration. Therefore, both energy transfer rate between Mn^{4+}-Mn^{4+} and the probability of energy transfer to luminescent killer sites increase. Consequently, the lifetimes are shortened as the increasing Mn^{4+} concentration.

3.3 Low temperature PL and decay analysis

The emission spectra of $La_3GaGe_5O_{16}$:0.25%Mn^{4+} sample is displayed within the temperature range of 10-300K in Figure 9. Two dominant, sharper peaks (B, D) and shoulder band (C) are observed in 10 K luminescence spectrum. Obviously, the luminescent intensities of these emission peaks (B, C and D) decrease along with increasing temperature. When comparing these emission spectra at different temperature, the abnormal anti-Stokes shoulder peak (A) grows with the temperature increasing. The abnormal phenomenon should be attributed to the thermal vibration of the host. The emission originates from the spin-forbidden $^2E \rightarrow {}^4A_2$ transition, giving rise to a long lifetime in a millisecond range. In other words, the electrons will stay in the ^2E excited state for a long time on account that the transition from the ^2E excited state to the $^4A_2$ ground state is spin-forbidden transition. Therefore, the electrons in ^2E state would be coupled with the lattice due to the thermal vibration along with the temperature growing, and then jumping from the lower vibrational energy level to the higher one until the electron distribution

reaches balance in these two levels. Afterwards, the shoulder peak appears and grows along with the temperature increasing, but the others are fading continuously.

We further measured the decay curves of the Mn^{4+} emission at 660 nm of $La_3GaGe_5O_{16}$:0.25%Mn^{4+} over the temperature range from 77 to 300K (see in Figure 10). At temperature up to 300K, all the decay curves of $La_3GaGe_5O_{16}$:0.25%Mn^{4+} is well fitted with the double-exponential equation as follows:

$$I(t) = A_1\exp(-\frac{t}{\tau_1}) + A_2\exp(-\frac{t}{\tau_2}) \qquad (8)$$

where τ_1 and τ_2 are the decay times for the short and long decay components; A_1 and A_2 are the fitting constants, respectively. The fitting results of all decay curves are listed in table 1. The results show clearly that either τ_1 or τ_2 decreases all the time along with increasing temperature.The decrement of the Mn^{4+} lifetime is also caused by the thermal vibration.

3.4 Quenching of High-Temperature Mn^{4+} PL

In order to investigate the influence of high temperature on the PL of $La_3GaGe_5O_{16}$:*x*Mn^{4+} phosphor, we measured the PL spectra of $La_3GaGe_5O_{16}$:0.25%Mn^{4+} upon excitation at 330 nm and 465 nm at different temperature. Figure 11 depicts the temperature dependence of Mn^{4+} PL integrated intensity under different excitation schemes upon the the circular testing processes of heating and cooling over the temperature range from 300 to 573K. The intensity is in integrated over the spectral range of 600 to 750 nm and it is normalized as compared to the case at 300 K. All the graphs give the similar trend regardless of whether UV or blue excitation was employed. Usually, the emission intensity of $La_3GaGe_5O_{16}$:0.25%Mn^{4+} decreases all the way along with the temperature growing. For whether UV or blue excitation, the quenching temperatures T_{50}, defined as the temperature at which the emission intensity is half of its original value, are determined to be about 423 K. When the temperature decreases from 573K to 300K, the intensity

of the emission almost recovers to the initial state, so the quenching and recovery are reversible considering the random errors of measurement. Therefore, the heating and cooling experiments imply no severe thermal degradation for $La_3GaGe_5O_{16}$:$x$$Mn^{4+}$ phosphors.

Furthermore, to further verify the origin of the temperature-dependent emission intensity (I_T), the activation energy (ΔE) can be calculated by the Arrhenius equation [18]:

$$I_t = \frac{I_0}{1 + A\exp(-\frac{\triangle E}{\kappa T})} \quad (9)$$

where I_0 is the initial intensity, I_T is the emission intensity at different temperature (T), ΔE is the activation energy for thermal quenching, A is the frequency factor, and κ is the Boltzmann constant ($\kappa=8.62\times10^{-5}eV\cdot K^{-1}$). According to the equation (9), the activation energy (ΔE) can be calculated to be ~0.105eV, which is close to that of promising deep red phosphors $Sr_4Al_{14}O_{25}:Mn^{4+}$[18] and $CaAl_4O_7:Mn^{4+}$[22]. For practical application in WLEDs, the quantum efficiency (QE) of the $La_3GaGe_5O_{16}:Mn^{4+}$ phosphor should be considered. Therefore, the QE of $La_3GaGe_5O_{16}:Mn^{4+}$ phosphor were 68% and 31% upon excitation at 332 nm and 467 nm, respectively.

The thermal quenching rationale can be explained by the configuration coordinate scheme, as shown in Figure 11(d). After excitation from the ground $^4A_2$ state to the $^4T_2$, corresponding to the blue absorption, nonradiative relaxation to the lowest excited state ^2E occurs, then electrons of ^2E transit to the ground state $^4A_2$ in radiative way, leading to the characteristic emission of Mn^{4+} ions. However, thermal excitation from ^2E occurs along with the temperature increasing. This excitation can occur via the crossover point of the states of $^4A_2$ and ^2E, resulting in nonradiative transition to the ground state $^4A_2$.

4. Conclusion

In summary, we prepared a new non-rare-earth red phosphor $La_3GaGe_5O_{16}:Mn^{4+}$ successfully by the simple solid-state reaction method. The diffuse and excitation spectra both present the broad absorption band from 250 to 550 nm, which is agreement with the wavelength of the UV and blue LEDs. This phosphor $La_3GaGe_5O_{16}:Mn^{4+}$ gives a bright red emission under excitation at either UV or blue light. The crystal field strength (Dq) and the Racah parameters (B and C) of the $La_3GaGe_5O_{16}$ host show that the nephelauxetic effect has an effect on the luminescence of Mn^{4+}. The optimal doping concentrations of Mn^{4+} in $La_3GaGe_5O_{16}:Mn^{4+}$ is about 0.25%. We also investigate the thermal stability and the quantum efficiency (QE) of $La_3GaGe_5O_{16}:Mn^{4+}$ phosphor. These results indicate $La_3GaGe_5O_{16}:Mn^{4+}$ can be promising as a potential candidate for the application in white LEDs. We aim to improve the performance of luminous efficacy of the $La_3GaGe_5O_{16}:Mn^{4+}$ in future by locally modifying composition around Mn^{4+} and optimizing morphological properties.

ACKNOWLEDGEMENTS

This work is supported by the National Natural Science Foundation of China (No. 21471038) and the National High Technology Research and Development Programs of China (2013AA03A101).

REFERENCES

(1). E. F. Schubert, and J. K. Kim, "Solid-state light sources getting smart ," *Science*, **308**[5726]1274-1278(2005).

(2). H.A. Höppe, Angew. "Recent Developments in the Field of Inorganic Phosphors," *Chem. Int. Ed*., **48**[20]3572-3582(2009).

(3). H. Daicho,T. Iwasaki, K. Enomoto,Y. Sasaki,Y. Maeno, Y. Shinomiya, S. Aoyagi, E. Nishibori, M. Sakata, H. Sawa, S. Matsuishiand, H. Hosono, "A novel phosphor for glareless white light-emitting diodes"*Nat. Commun*., 3,1132-(October 2012).

(4). D.Wen, J.Feng, J.Li, J.Shi, M.Wu and Q. Su, "$K_2Ln(PO_4)(WO_4):Tb^{3+},Eu^{3+}$ (Ln = Y, Gd and Lu) phosphors: highly efficient pure red and tuneable emission for white light-emitting diodes," *J. Mater. Chem. C*, **3**[48]2107-2114(2015).

(5). M. Y. Peng and L.Wondraczek, "Photoluminescence of $Sr_2P_2O_7:Bi^{2+}$ as a red phosphor for additive light generation," *Opt. Lett*., **35**[15]2544-2546(2010).

(6). F. W. Kang , Y. Zhang , and M. Y. Peng, "Controlling the Energy Transfer via Multi Luminescent Centers to Achieve White Light/Tunable Emissions in a Single-Phased X2-Type $Y_2SiO_5:Eu^{3+},Bi^{3+}$ Phosphor For Ultraviolet Converted LEDs," *Inorg. Chem*., **54**[4]1462-1473(2015).

(7). S. A. Zhang, Y.H. Hu, L. Chen, X.J. Wang, G.F.Ju, Y. Fan, "Photoluminescence properties of $Ca_3WO_6:Eu^{3+}$ red phosphor," *J. Lumin*, **2013**, 142,116-121 (October 2013).

(8). J. Oh , H. Kang , Y. Eo , H. Park and Y. Do, "Synthesis of narrow-band red-emitting $K_2SiF_6:Mn^{4+}$ phosphors for a deep red monochromatic LED and ultrahigh color quality warm-white LEDs," *J. Mater. Chem. C*, **3**[3]607-615(2015).

(9). M.M. Shang, C.X. Li, J. Lin, "How to produce white light in a single-phase host? " *Chem.Soc.Rev*.,**43**[5]1372-1386(2014).

(10). P. A. Tanner, "Some misconceptions concerning the electronic spectra of tri-positive europium and cerium," *Chem. Soc. Rev*.**42**[12]5090-5101(2013).

(11). F. Kang, X.Yang, M. Peng, L.Wondraczek,Z. Ma, Q. Zhang, J. Qiu, "Red photoluminescence from Bi^{3+} and the influence of the oxygen-vacancy perturbation in

ScVO4: A combined experimental and theoretical study," *J. Phys. Chem. C*,**118**[14] 7515-7522(**2014**).

(12). C.C. Lin, R.S. Liu, "Advances in phosphors for light-emitting diodes," *J. Phys. Chem. Lett.* **2**[11]1268-1277(2011).

(13). Y.Q. Li, J. Van Steen, J. Van Krevel, G. Botty, A. Delsing, "ZnB2O4:Bi3+,Eu3+:a highly efficient, red-emitting phosphor," *Opt Express*.,**18**[3]2946-51(2010).

(14). K. Uheda, N. Hirosaki, Y. Yamamoto, A. Naito, T. Nakajima, H. Yamamoto, "Luminescence properties of a red phosphor, $CaAlSiN_3:Eu^{2+}$, for white light-emitting diodes."*Electrochem. Solid-state Lett.* **9**[4]H22-H25(2006).

(15). P. F. Smet, A.B, Parmentier, D. Poelman, "Selecting conversion phosphors for white light-emitting diodes,"*J. Electrochem. Soc*. **158**[6]R37-R54(2011).

(16). H.M. Zhu, C.C, Lin, W.Q. Luo, S. T. Shu, Z.G. Liu, Y. S. Liu, J. T. Kong, E. Ma, Y.G. Cao, R.S. Liu, X.Y. Chen, "Highly efficient non-rare-earth red emitting phosphor for warm white light-emitting diodes,"*Nat. Commun.* **2014**, 5, 4312.

(17). S. Okamoto, H. Yamamoto,"Photoluminescence Properties of $BaMgAl_{10}O_{17}$ Doped with High Concentration of Mn^{2+} for Blue-LED-Based Solid-State Lighting" *J. Electrochem. Soc.*,**158**[11]J59-J63(2010).

(18). M. Y. Peng, X. W. Yin, P. A.Tanner, M.G.Brik, and P. F. Li, "Site Occupancy Preference, Enhancement Mechanism, and Thermal Resistance of Mn^{4+} Red Luminescence in $Sr_4Al_{14}O_{25}:Mn^{4+}$ for Warm WLEDs,"*Chem. Mater.*, **27**[8]2938-2945(2015).

(19). M. Y. Peng, X. W. Yin, P. A.Tanner, C. Liang, P. F. Li, Q.Y. Zhang, and J.R. Qiu, "Orderly□Layered Tetravalent Manganese□Doped Strontium Aluminate $Sr_4Al_{14}O_{25}$:

Mn^{4+}: An Efficient Red Phosphor for Warm White Light Emitting Diodes," *J. Am. Ceram. Soc.*,**96**[9]2870-2876(2013).

(20). B. Wang, H. Lin, J. Xu, H. Chen, and Y.S . Wang, "$CaMg_2Al_{16}O_{27}$: Mn4+-based Red Phosphor: A Potential Color Converter for High-Powered Warm W-LED."*ACS Appl. Mater. Interfaces*, **6**[24]22905-22913(2014).

(21). L.L. Meng, L.F. Liang, and Y.X. Wen, "Deep red phosphors $SrMgAl_{10}O_{17}:Mn^{4+}$, M (M= Li^+, Na^+, K^+, Cl^-) for warm white light emitting diodes."*J. Mater. Sci. Mater. Electron*, **25**[6] 2676-2681(2014).

(22). P. Li, M. Peng, X. Yin, Z.Ma,G. Dong, Q. Zhang, and J. Qiu, "Temperature dependent red luminescence from a distorted Mn^{4+} site in $CaAl_4O_7:Mn^{4+}$," Opt. express, **21**(16), 18943-18948(2013).

(23). T. Murata, T, Tanoue, M. Iwasaki, K. Morinaga, T. Hase, "Fluorescence properties of Mn^{4+} in $CaAl_{12}O_{19}$ compounds as red-emitting phosphor for white LED,"*J. Lumin*, **114**, 207-212(2005).

(24). G.Adiwidjaja, M. Broeker, C. Claus, K. Friese, K.H. Klaska, O. Jarchow, M.Ruks, I.Wozniak, "Structure of the compounds $La_3AlGe_5O_{16}$, $La_3GaGe_5O_{16}$ and $Ce_3GaGe_5O_{16}$," Zeitschrift für Kristallographie, **213**[4] 223-227(1998).

(25). J. Zhou and Z.G. Xia, "Synthesis and near-infrared luminescence of $La_3GaGe_5O_{16}:Cr^{3+}$ phosphors,"*RSC Adv.*, **4**[86]46313-46318(2014).

(26). J. Zhou and Z.G. Xia, "Multi-color emission evolution and energy transfer behavior of $La_3GaGe_5O_{16}:Tb^{3+}$, Eu^{3+} phosphors," *J. Mater. Chem. C*, **2**[34]6978-6984(2014).

(27). B. Viana, A. M. Lejus, D. Vivien, V. Poncon, G. Boulon, "Synthesis, ESR investigation, and optical properties of the potential vibronic laser material $LaMgAl_{11-x}Cr_xO_{19}$," *J. Solid. State. Chem.***71**[1]77-86(1987).

(28). V. Singh, R. Chakradhar, J. L. Rao, D.K. Kim, "Photoluminescence and EPR studies of Cr-doped hibonite ($CaAl_{12}O_{19}$) phosphors," *Solid. State. Sci.* **10**[11]1525-1532(2008).

(29). P. A. Tanner, and Z. Pan, "Luminescence Properties of Lanthanide and Transition Metal Ion-Doped Ba_2LaNbO_6: Detection of MnO_6^{8-} and CrO_6^{9-} Clusters," *Inorg. Chem.*, **48**[23] 11142-11146(2009).

(30). M.J. Reisfeld, N. A. Matwiyof, L. B. Aspery, "The electronic spectrum of cesium hexafluoromanganese (IV)," *J. Mol. Spectrosc.* **39**[1]8-20(1971).

(31). B. Henderson, G. F. Imbrush, Optical Spectroscopy of Inorganic Solids. Clarendon Press, Oxford, 1989.

(32). G. Blasse, "Energy transfer between inequivalent Eu^{2+} ions,"*J. Solid State Chem.*, **62**[2]207-211(1986).

(33). D. L. Dexter, "A theory of sensitized luminescence in solids,"*J. Chem. Phys.*, **21**[5] 836-840(1953).

Figure Captions

Figure 1. View of the structure of $La_3GaGe_5O_{16}$ from a-projection, and different cation (Ga, and Ge) coordination polyhedra are shown, respectively.

Figure 2. XRD patterns of $La_3GaGe_5O_{14}$:*x*Mn^{4+} (*x*=0.05%, 0.15%, 0.25%, 0.35% and 0.50%) along with $La_3GaGe_5O_{14}$ host

Figure 3.(a-d) SEM of the as-synthesized $La_3GaGe_5O_{16}$:Mn^{4+} red phosphors. The scale bar in SEM images is at the bottom of the picture and the enlargement factors of the particles are 200, 500, 5000, and 10000 times, respectively.

Figure 4. The representative diffuse reflection spectra of $La_3GaGe_5O_{16}$ host and $La_3GaGe_5O_{16}$:*x*Mn^{4+} (*x*=0.05%, 0.15%, and 0.25%)

Figure 5. PLE (λ_{em}=660 nm) and PL (λ_{ex}=330 nm) spectra of $La_3GaGe_5O_{16}$:0.25%Mn^{4+} at room temperature

Figure 6. (a) Energy level diagram of Mn^{4+} corresponding to the PLE (λ_{em}=660 nm); (b) Tanabe-Sugano energy level diagram for Mn^{4+} in the octahedral site of $La_3GaGe_5O_{16}$ host

Figure 7. (a) PLE (λ_{em}=660 nm) and (b) PL (λ_{ex}=330 nm) spectra of $La_3GaGe_5O_{16}$:*x%*Mn^{4+} samples (*x*=0.05, 0.15, 0.25, 0.35, and 0.50); (c) PL intensity of Mn^{4+} as a function of Mn^{4+} doping intensity in the samples; (d) dependence of log(I/*x*) on log(x) based on the Eqn. 7

Figure 8. Room temperature decay lifetime curves of $La_3GaGe_5O_{16}$:*x%*Mn^{4+} samples with different Mn^{4+} content (*x*=0.05, 0.15, 0.25, 0.35, and 0.50)

Figure 9. Emission spectra (λ_{ex}=330 nm) of $La_3GaGe_5O_{16}$:0.25%Mn^{4+} sample measured within the temperature range of 10-300K.

Figure 10. Decay curves (λ_{ex}=330 nm, λ_{em}=660nm) of $La_3GaGe_5O_{16}$:0.25%Mn^{4+} sample measured within the temperature range of 77-300K

Figure 11. (a-b) Temperature-dependent relative emission intensity of $La_3GaGe_5O_{16}$:0.25%Mn^{4+} sample in heating (blue curve) and cooling (black curve) processes under UV and blue light excitation schemes;The solid red curves are fitted to the heating process by eqn(9); (c) the PL spectra of $La_3GaGe_5O_{16}$:0.25%Mn^{4+} upon excitation at 330 nm at different temperature; (d) the configuration coordinate diagram of $La_3GaGe_5O_{16}$:0.25%Mn^{4+} under excitation with blue light.

Table 1. Lifetimes of $La_3GaGe_5O_{16}$:0.25%Mn^{4+} measured in the temperature range from 77 to 300K

$La_3GaGe_5O_{16}$:0.25%Mn^{4+}	77K	100K	150K	200K	250K	300K
τ_1 (ms)	0.795	0.626	0.584	0.368	0.339	0.184
τ_2 (ms)	1.971	1.694	1.852	1.458	1.260	0.966

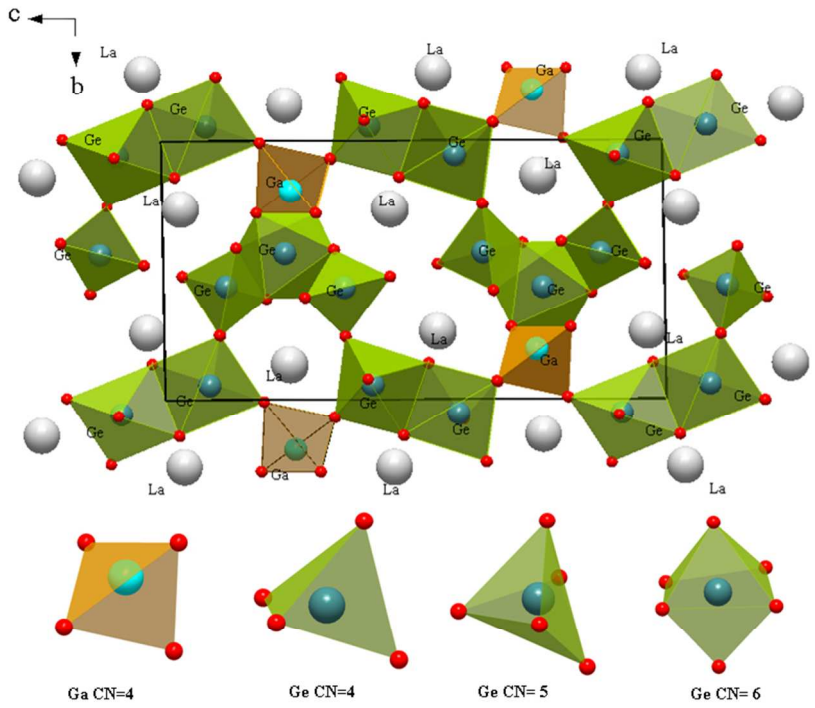

254x190mm (96 x 96 DPI)

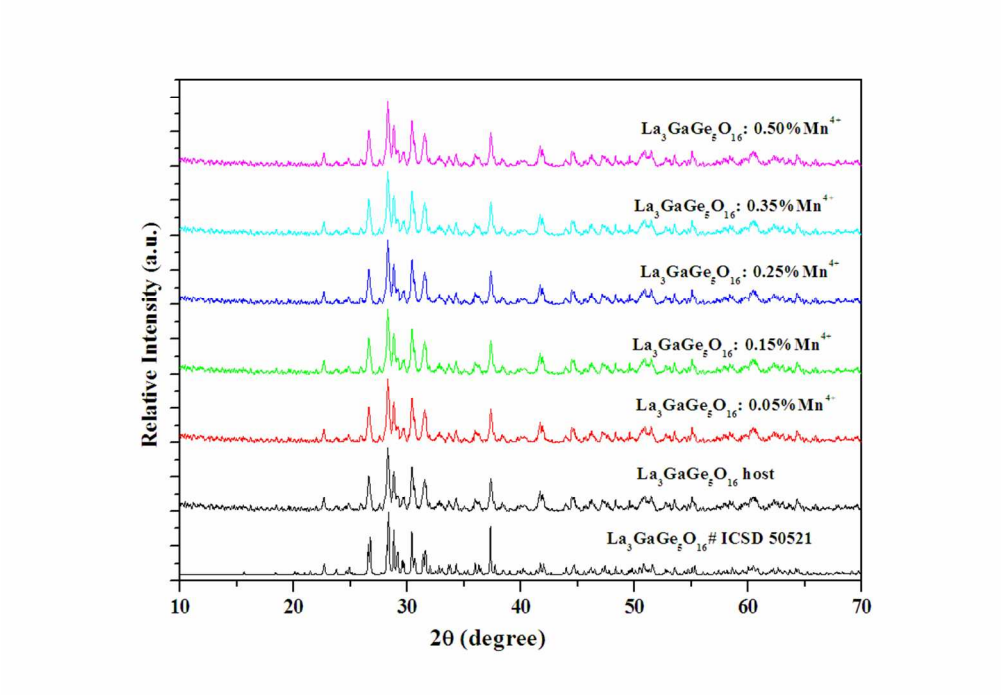

Figure 2. XRD patterns of La3GaGe5O14:xMn4+ (x=0.05%, 0.15%, 0.25%, 0.35% and 0.50%) along with La3GaGe5O14 host
192x134mm (150 x 150 DPI)

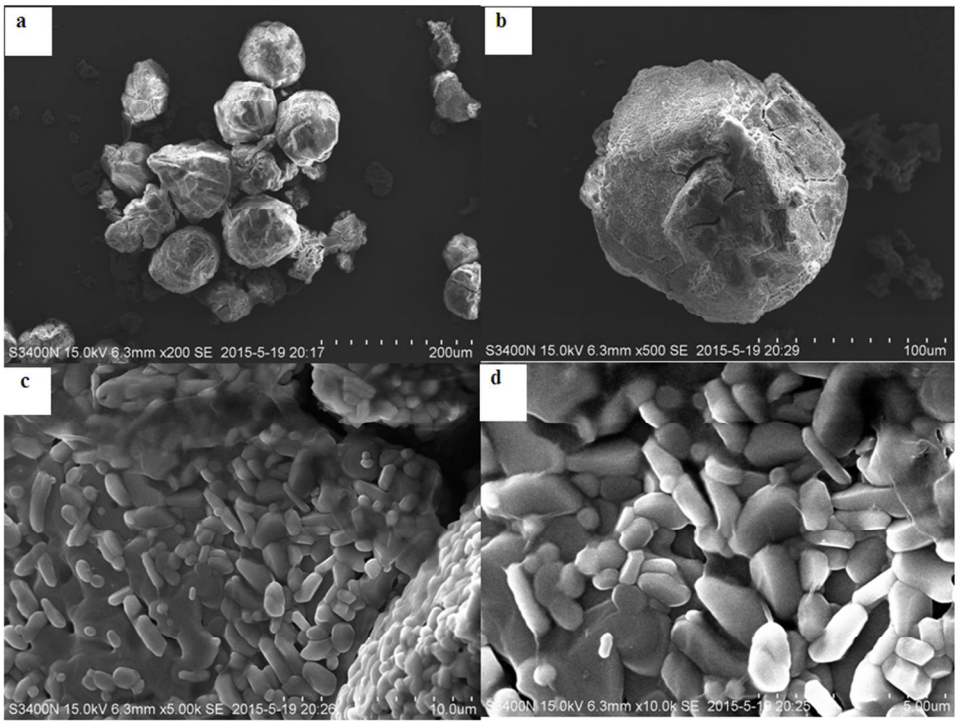

Figure 3.(a-d) SEM of the as-synthesized La3GaGe5O16:Mn4+ red phosphors. The scale bar in SEM images is at the bottom of the picture and the enlargement factors of the particles are 200, 500, 5000, and 10000 times, respectively.
254x190mm (96 x 96 DPI)

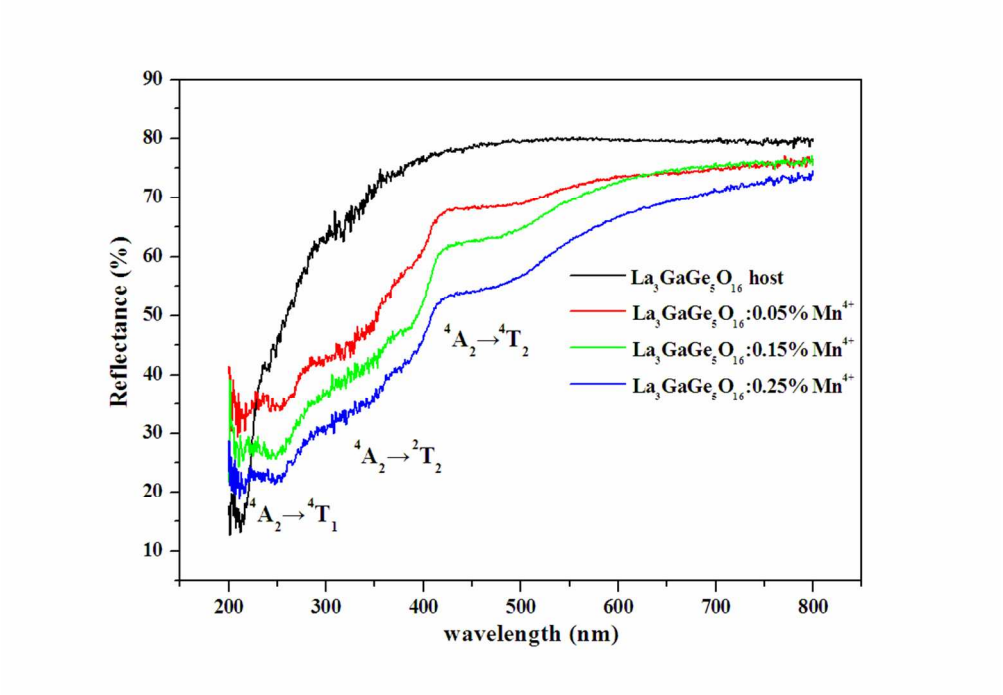

Figure 4. The representative diffuse reflection spectra of La3GaGe5O16 host and La3GaGe5O16:xMn4+ (x=0.05%, 0.15%, and 0.25%)
192x134mm (150 x 150 DPI)

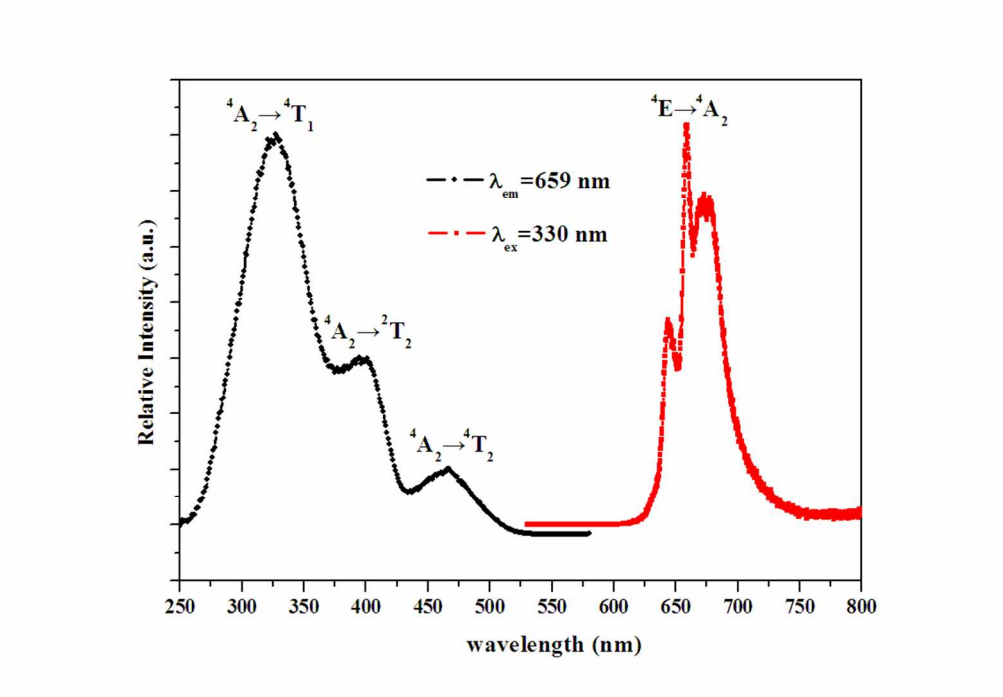

Figure 5. PLE (λem=660 nm) and PL (λex=330 nm) spectra of La3GaGe5O16:0.25%Mn4+ at room temperature
192x134mm (150 x 150 DPI)

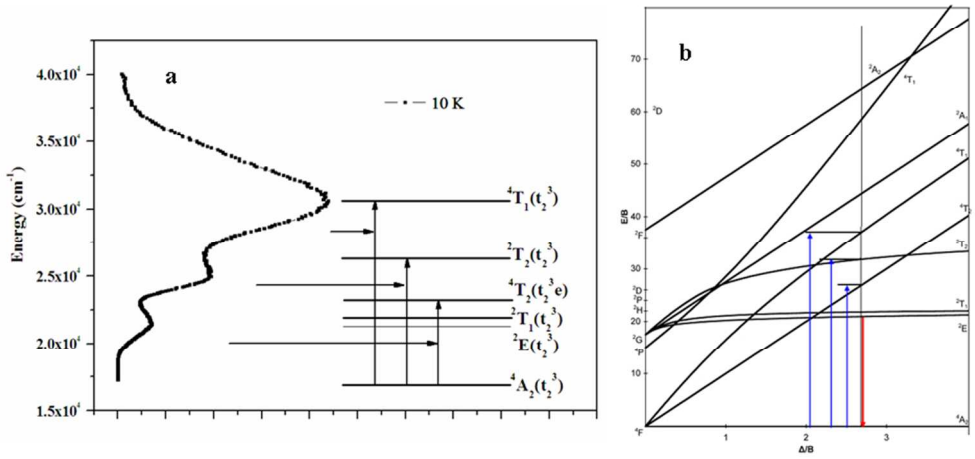

Figure 6. (a) Energy level diagram of Mn4+ corresponding to the PLE (λem=660 nm); (b) Tanabe-Sugano energy level diagram for Mn4+ in the octahedral site of La3GaGe5O16 host
254x190mm (96 x 96 DPI)

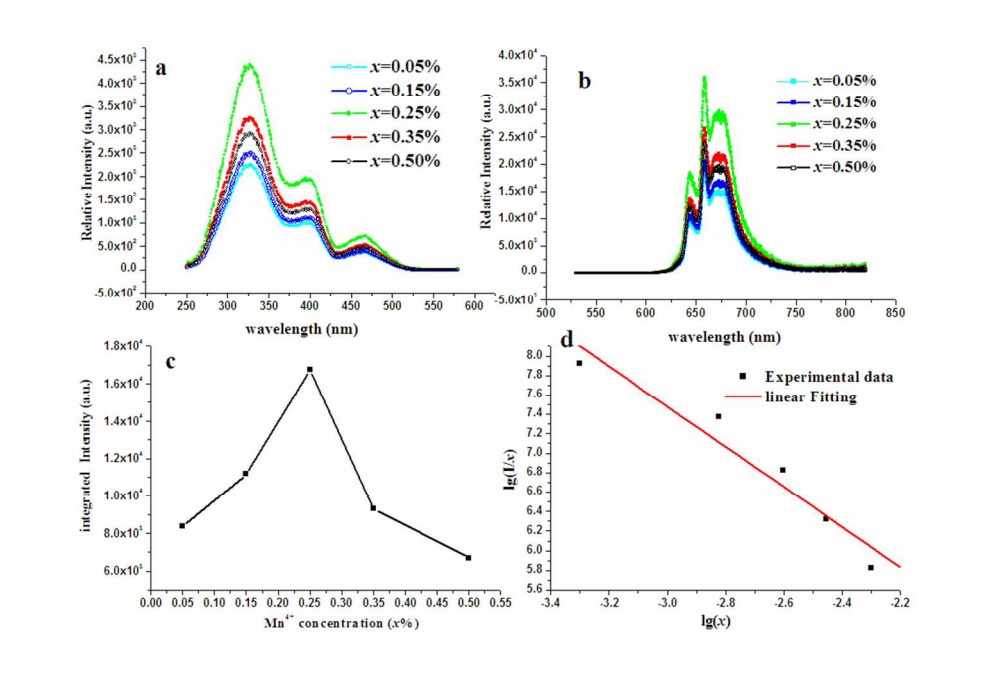

Figure 7. (a) PLE (λem=660 nm) and (b) PL (λex=319 nm) spectra of La3GaGe5O16:x%Mn4+ samples (x=0.05, 0.15, 0.25, 0.35, and 0.50); (c) PL intensity of Mn4+ as a function of Mn4+ doping intensity in the samples; (d) dependence of log(I/x) on log(x) based on the Eqn. 7
192x134mm (150 x 150 DPI)

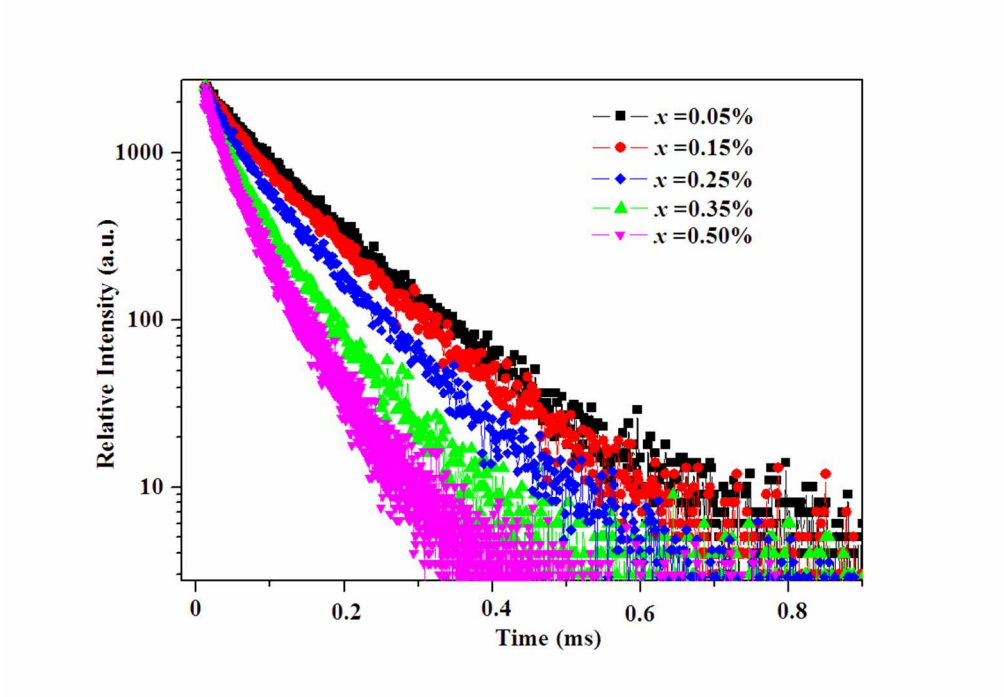

Figure 8. Room temperature decay lifetime curves of La3GaGe5O16:x%Mn4+ samples with different Mn4+ content (x=0.05, 0.15, 0.25, 0.35, and 0.50)
192x134mm (150 x 150 DPI)

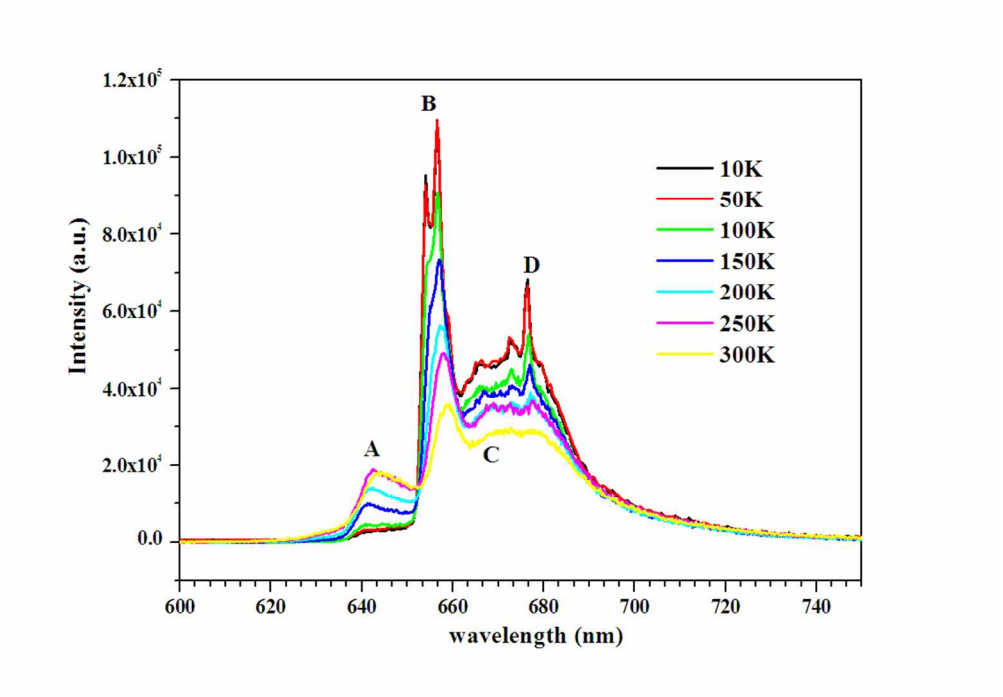

Figure 9. Emission spectra （λex=330 nm) of La3GaGe5O16:0.25%Mn4+ sample measured within the temperature range of 10-300K.
192x134mm (150 x 150 DPI)

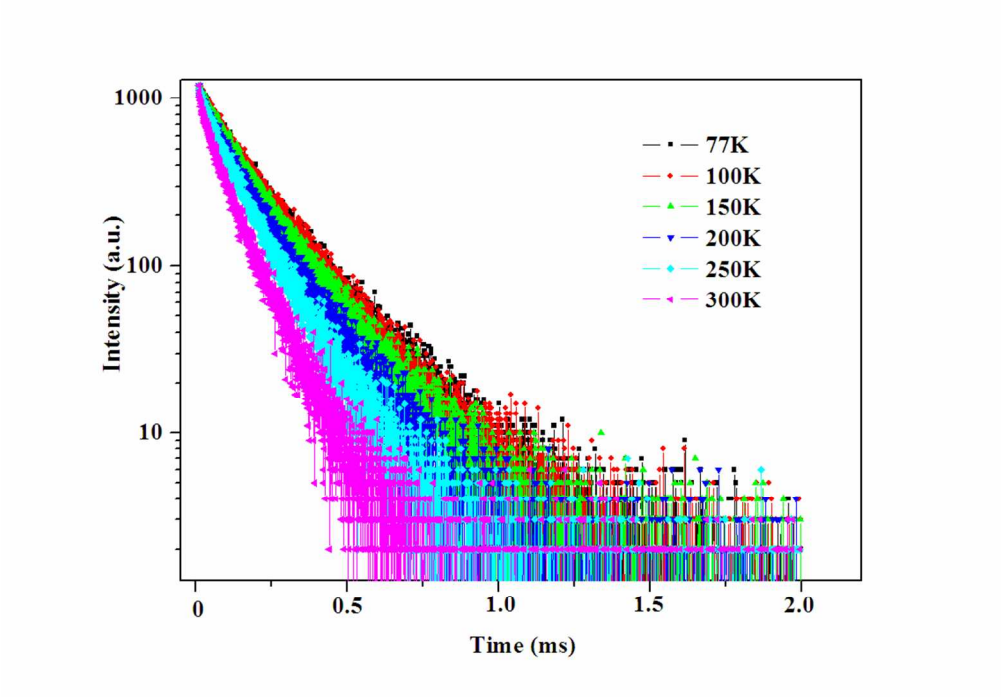

Figure 10. Decay curves (λex=330 nm, λem=660nm) of La3GaGe5O16:0.25%Mn4+ sample measured within the temperature range of 77-300K
192x134mm (150 x 150 DPI)

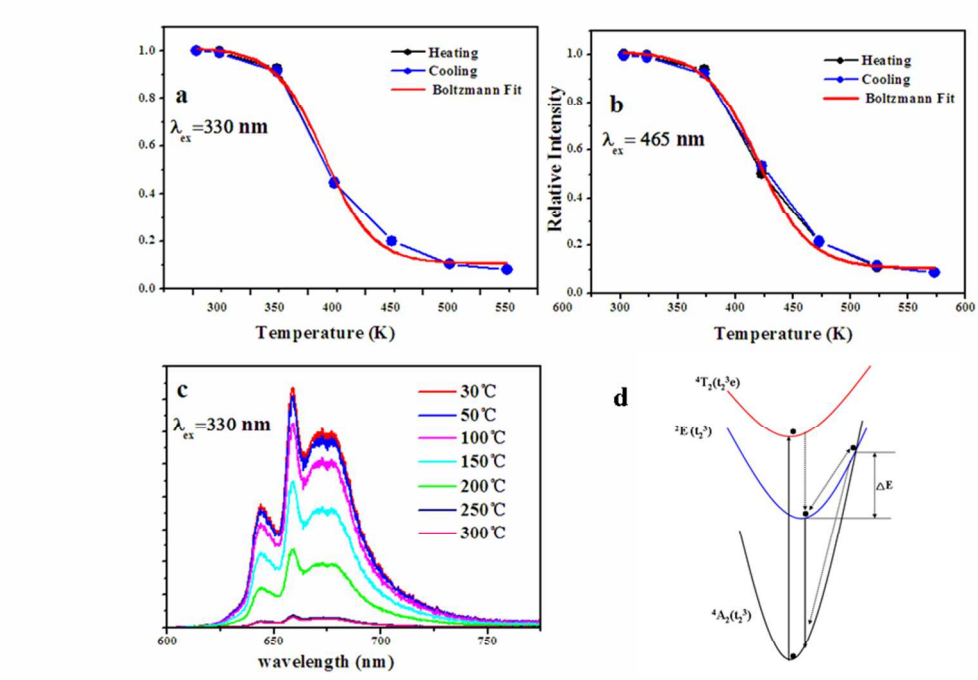

254x190mm (96 x 96 DPI)